Progress In Electromagnetics Research, PIER 85, 409–424, 2008

A SINGLE-FEED CYLINDRICAL SUPERQUADRIC DIELECTRIC RESONATOR ANTENNA FOR CIRCULAR POLARIZATION

S. H. Zainud-Deen, H. A. Malhat, and K. H. Awadalla

Faculty of Electronic Engineering
Menoufia University
Egypt

Abstract—Circularly polarized superquadric dielectric resonator antenna is investigated. A single coaxial probe is used to excite circularly polarized patterns. Finite element method is used to analyze the problem. Different aspect ratios of the superquadric dielectric resonator cross section for each squareness parameter for circular polarization are calculated.

1. INTRODUCTION

The dielectric resonator antennas (DRAs) became attractive to antenna designers since about 20 years ago [1–5]. DRA has many advantages such as small size, low transmission loss and ease of integration with other active or passive MIC components. In addition, DRAs exhibit a relatively large bandwidth ($\sim 10\%$ for $\epsilon_r \sim 10$), while the patch antenna has a typical bandwidth of only 1–3%. Moreover, DRAs avoid the inherent disadvantage of patch antennas, such as high conduction loss at millimeter wave frequencies, and low efficiency due to surface wave excitation. In its simplest form, a dielectric resonator antenna is normally made of high-permittivity material and is located on a conducting ground plane. DRA can be versatile in shape and exhibit many resonant modes [6–9] which have different radiation characteristics. A variety of different feeding mechanisms are available, including excitation by probes [10], slots [11], microstrip lines [12], dielectric image guides, and coplanar lines [13], and the various antenna characteristics such as input impedance, bandwidth, and radiation patterns can be controlled by choosing the dielectric constant, the dimensions of the dielectric resonator material and the feeding mechanism.

Circular polarization has been used in some mobile satellite communications and vast number of communication systems. A typical technique for producing circular polarization is by using the feeding structure to excite two orthogonal linearly polarized modes with a 90° phase difference. In [14], the operation of circular polarized dielectric resonant antenna has been proposed in which circular polarization operation was accomplished by using two unequal cross slots to couple energy from microstrip line to a simple DRA. Because their lengths were unequal, the two near-degenerate orthogonal modes of equal amplitude and 90° phase difference were excited with a relatively less polarization purity. Recently, a single-fed elliptical dielectric resonator antenna is designed for circular polarization [15].

In this paper, a single coaxial probe is used to excite a superquadric dielectric resonator antenna for circular polarization. The radiation characteristics of the superquadric dielectric resonator antenna are investigated using the Finite Element Method for the first time. The dimensions of the antenna and length of the feeding probe are designed for circular polarization.

2. THE FINITE ELEMENT METHOD

The finite element method (FEM) has become an invaluable tool for the analysis of electromagnetic problems with complex geometries. In particular, the three-dimensional (3D) FEM allows for the rigorous analysis of a broad range of practical structures [16–20]. The routine use of the FEM in design problems can, however, become cumbersome due to the vast computational resources often required. The advantages of the FEM are [21]:

- Sparse matrices result (as opposed to MoM for which dense matrices result). Sparse matrices allow the application of a wide range of fast matrix solvers.
- Its application involves discretization of the computational domain, and therefore is adaptable to a wide range of geometries and material variations.

Figure 1 illustrates a generic problem. The computational region is the enclosed volume, Ω. The vector wave equation is the starting point for the FEM solution

$$\nabla \times \left(\frac{\nabla \times \bar{E}}{\mu_r} \right) - k^2 \varepsilon_r \bar{E} = -jkZ\bar{J} - \nabla \times \left(\frac{\bar{J}_m}{\mu_r} \right)$$
$$L\left(\bar{E}\right) = \bar{f} \tag{1}$$

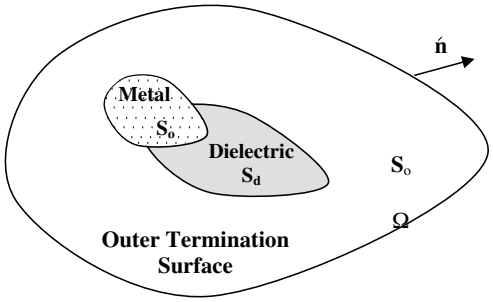

Figure 1. The problem configuration.

where Z, J_m, and k are the characteristic wave impedance, the current density and the wave number respectively. A testing procedure is used similar to the method of moments. Each side is multiplied by a testing (weighting) function, and integrated. Using the inner product notation

$$\left\langle \bar{A}, \bar{W} \right\rangle = \int_{\Omega} \bar{A} \cdot \bar{W} d\Omega \tag{2}$$

where $\bar{W}$ is the test function and $\bar{A}$ is a field or current. Ideally, the two sides of the wave equation should be equal and the difference is zero. In practice the difference will not be zero due to the expansion of the current distribution into finite number of basis functions with unknown coefficients, so we minimize the functional

$$F\left(\bar{E}\right) = \left\langle L\left(\bar{E}\right), \bar{W} \right\rangle - \left\langle \bar{f}, \bar{W} \right\rangle \tag{3}$$

The finite element method of the problem involves basically four steps [22]:

- Discretizing the solution region into a finite number of sub-regions or elements.
- Deriving governing equations for a typical element.
- Assembling of all elements in the solution region.
- Solving the system of equations obtained.

In the finite element method, the radiation boundaries are used to simulate open problems that allow waves to radiate infinitely far into space. The waves are observed at the radiation boundary surface. More details about the finite element method can be found in [22].

3. ANTENNA STRUCTURE

Figure 2 shows the geometry of the cylindrical superquadric dielectric resonator antenna structure. The dielectric resonator antenna of height "h" and dielectric permittivity "ϵ_r" has a superquadric cross section area with aspect ratio "a/b" (major to minor axes ratio). The superquadric cross section curve is the locus of points satisfying the following equation [23],

$$\left(\frac{x}{a}\right)^{\nu} + \left(\frac{y}{b}\right)^{\nu} = 1 \quad x \le a, \text{ and } y \le b \tag{4}$$

where "a" and "b" are the semi-axes in the x and y directions respectively, and ν is a "squareness parameter" which controls the behavior of loop radius of curvature. The coordinates of any point on the curvature are given by,

$$\left.\begin{aligned} x &= a\psi(\beta)\cos\beta \\ y &= b\psi(\beta)\sin\beta \end{aligned}\right\} \tag{5}$$

where

$$\psi(\beta) = \left(|\sin\beta|^{\nu} + |\cos\beta|^{\nu}\right)^{-1/\nu}.$$

The parameter β is in the range $(0 \le \beta \le 2\pi)$. An important feature of this particular representation is the fact that equal divisions in the parameter β results in reasonably equal values of arc length for the sub-sectional segments. Figure 2(b) illustrates the superquadric geometry for $\nu = 2$, 3, and 10 and an aspect ratio of "a/b" $= 1.5$. Thus the superquadric loop allows modeling of different dielectric resonator configurations through the variation of parameters a, b, and ν starting

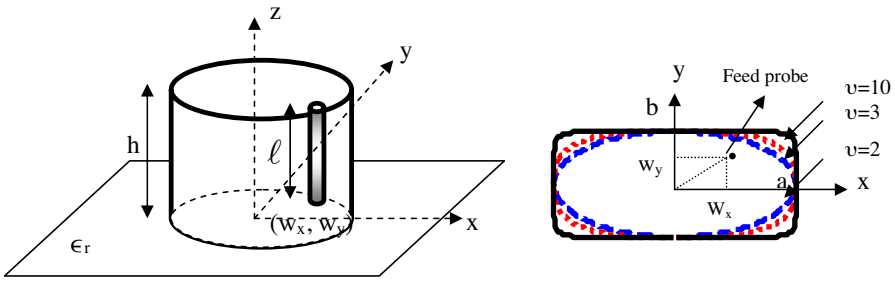

(a) 3D geometry (b) superquadric cross section

Figure 2. Geometry of the elliptic dielectric resonator antenna excited by a probe.

from circular (ellipse) to square (rectangular) cross sectional area. The feeding probe of length "ℓ" is embedded within the DRA at feed point (w_x and w_y). The DRA is mounted on an infinite size ground plane. As the squareness parameter "ν" and aspect ratio "a/b" have the most effect on the dielectric resonator antenna characteristics, through out the paper these parameters are studied to obtain the best circular polarization.

4. NUMERICAL RESULTS

To verify our analysis, a superquadric DRA with $\nu = 2$ (elliptical cross section) with major axis $a = 5.25\,\text{mm}$, $b = 3.5\,\text{mm}$, $h = 3.5\,\text{mm}$, $\epsilon_r = 12$, $\ell = 3\,\text{mm}$, feed probe radius of $0.25\,\text{mm}$, and feed probe location at ($2\,\text{mm}$, $2\,\text{mm}$) is simulated and compared with results in [15]. Figures 3 and 4 show comparison between the calculated input impedance and the reflection coefficients and that calculated in [15]. Figure 5 depicts the results of the axial ratio (AR) against frequency. Figure 6 shows the circular polarization components copolar and cross polar radiation patterns plotted at frequency $f = 9.28\,\text{GHz}$. The simulated results are in good agreement with the results in [15].

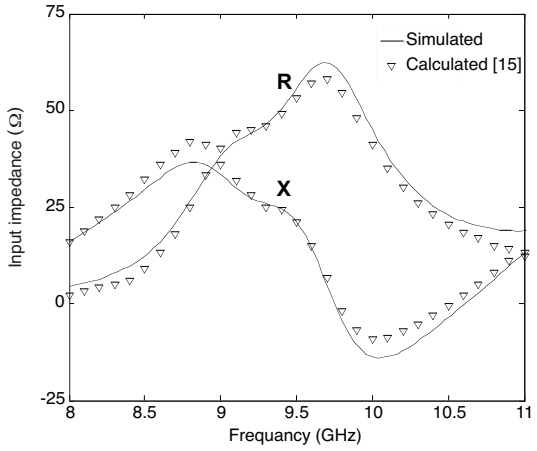

Figure 3. Input impedance of superquadric DRA.

In the following sections a parametric study is done for computing the best axial ratio for each superquadric case (ν, a/b) to obtain the widest bandwidth for circular polarization. The squareness parameter "ν" of the superquadric DRA is varied and taking the values (2, 4, and 10) which varies the DRA cross section shape from ellipse to

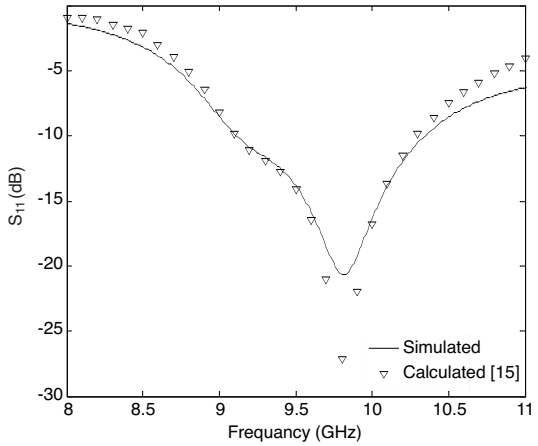

Figure 4. Reflection coefficient of superquadric DRA (relative to $50\,\Omega$ feed line).

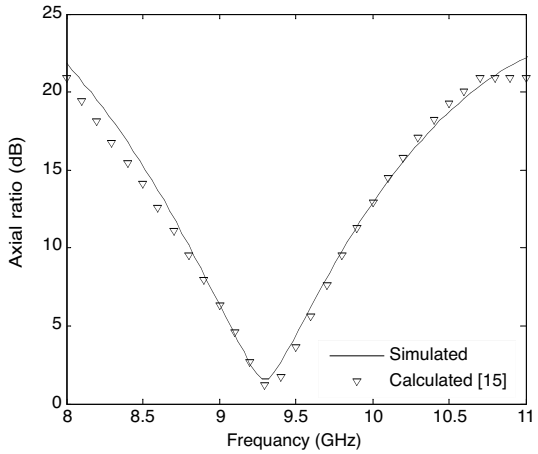

Figure 5. The axial ratio versus frequency of superquadric DRA ($\nu = 2$).

rectangular. The superquadric DRA feeding probe is located at (w_x, w_y) = (2 mm, 2 mm) just inside the dielectric. The axial ratio along the antenna axis is computed for a superquadric DRA with different aspect ratios (a/b). The minor axis $b = 3$ mm, $h = 3.5$ mm, $\epsilon_r = 12$, $\ell = 3$ mm, feed probe radius of 0.25 mm, and feed probe location at (2 mm, 2 mm). These dimensions are used to agree with that used in [15].

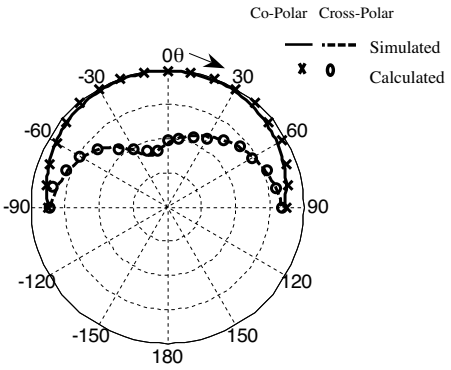

Figure 6. Computed circular polarization co-polar and cross-polar radiation pattern at the frequency that has best axial ratio at $f = 9.28\,\text{GHz}$.

Table 1. The different superquadric DRA at case (1).

Squareness parameter (ν)	**Aspect ratio** (a/b)	**Resonance frequency** (f_r) **GHz**
$\boldsymbol{\nu = 2}$	1.5	10.2
$\boldsymbol{\nu = 4}$	1.6	9.5
$\boldsymbol{\nu = 6}$	1.6	9.4
$\boldsymbol{\nu = 8}$	1.7	9.2
$\boldsymbol{\nu = 10}$	1.7	9.2

Table 2. The different superquadric DRA at case (2).

Squareness parameter (ν)	**Aspect ratio** (a/b)	**Resonance frequency** (f_r) **GHz**
$\boldsymbol{\nu = 2}$	1.4	10
$\boldsymbol{\nu = 4}$	1.5	9.2
$\boldsymbol{\nu = 6}$	1.5	9.1
$\boldsymbol{\nu = 8}$	1.6	8.9
$\boldsymbol{\nu = 10}$	1.7	8.7

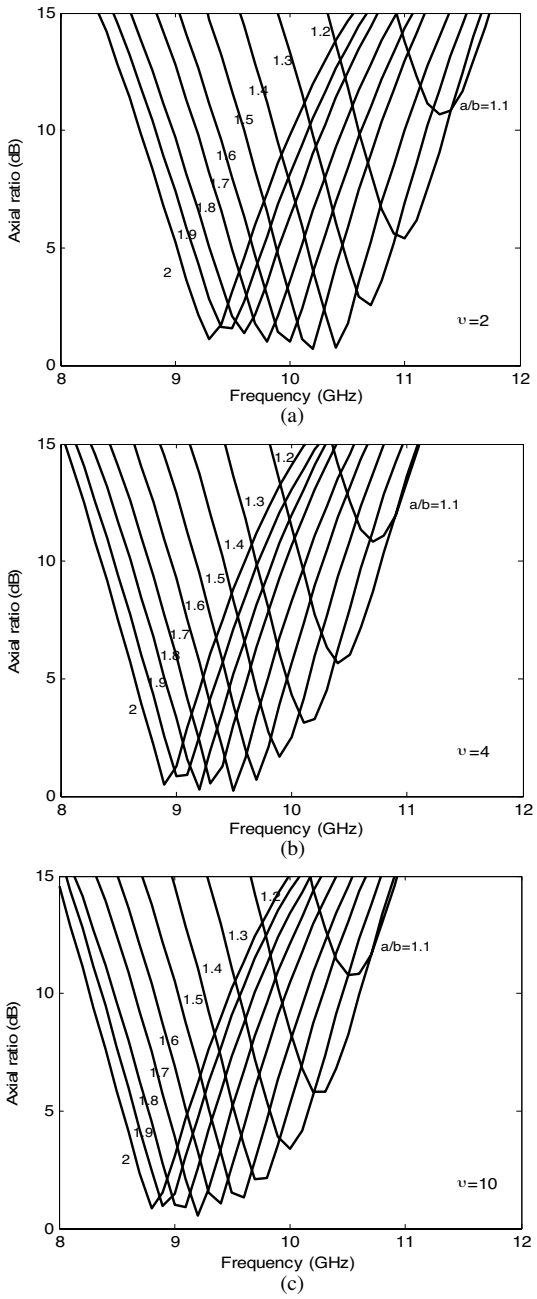

Figure 7. The axial ratio of superquadric DRA at different squareness parameter.

Figure 7 shows the axial ratio (AR) computed against frequency at different values of "ν". The resonant frequency decreased as the aspect ratio (a/b) increased when "ν" increased (going to be rectangular). Also the polarization axial ratio is poor when (a/b) is close to one. The major observation that at each "ν" there will be a certain value for aspect ratio (a/b) that gives the best axial ratio with the widest bandwidth for circular polarization. Figure 8 shows the best axial ratio (its minimum close to 0 dB) curve versus frequency for each "ν" and aspect ratio (a/b). For the same aspect ratio (a/b), increasing

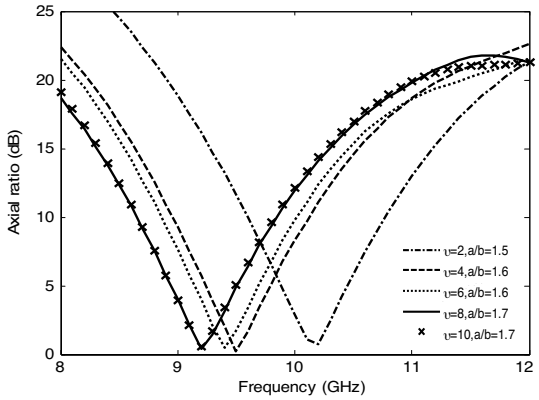

Figure 8. The best axial ratio of superquadric DRA at different squareness parameter.

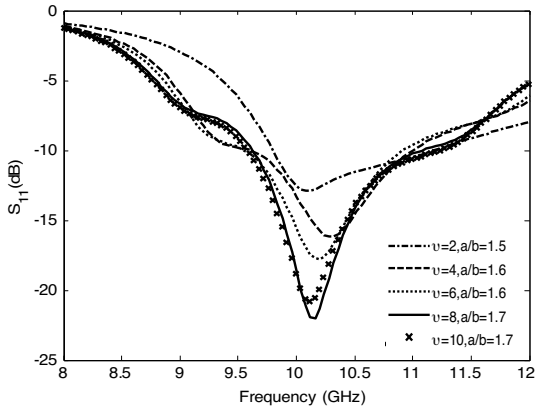

Figure 9. The reflection coefficients corresponding to best axial ratio of Figure 8.

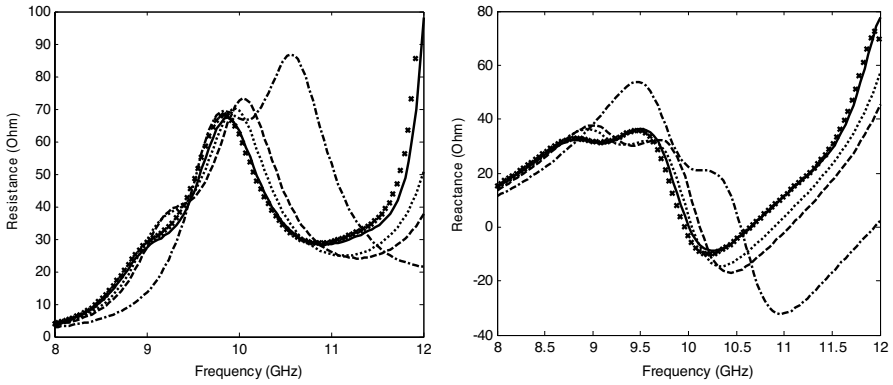

(a) Real part (b) Imaginary part

Figure 10. The input impedance corresponding to best axial ratio of Figure 8.

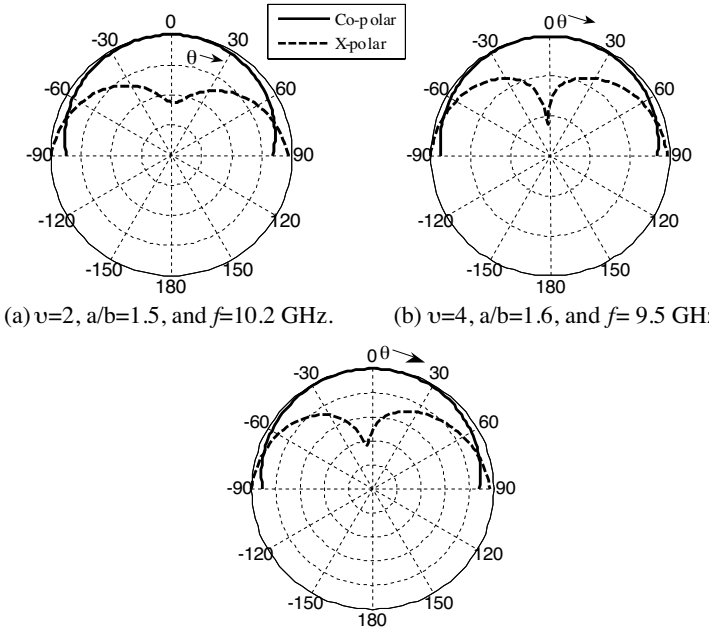

(a) υ=2, a/b=1.5, and *f*=10.2 GHz. (b) υ=4, a/b=1.6, and *f*= 9.5 GHz.

(c) υ=10, a/b=1.7, and *f* = 9.2 GHz.

Figure 11. Computed circular polarization copular and cross-polar radiation patterns at the frequency that has best axial ratio for each case, $h = 3.5\,\text{mm}$ and $L = 3\,\text{mm}$.

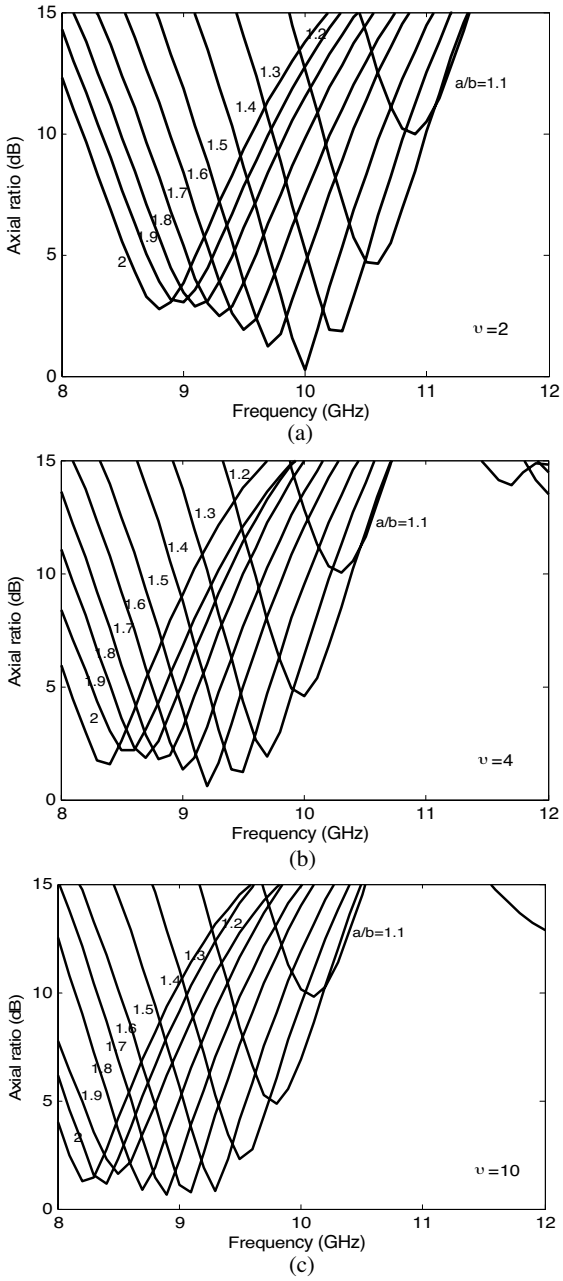

Figure 12. The axial ratio of superquadric DRA at different squareness parameter.

the squareness parameter (ν) leads to an increase in the volume of the cylinder with both "a" and "b" are kept constant, which also leads to a decrease in the resonant frequency of the cylinder. The corresponding reflection coefficient and input impedance for each case are shown in Figures 9 and 10 respectively. From Fig. 8 and Fig. 9 good impedance matching occurs depending on the definition of 2.5 dB:1 axial ratio or about 7.3 dB return loss [24] for different values of (ν) and the aspect ratio (a/b), i.e., both the axial ratio bandwidth (below 2.5 dB) and the impedance bandwidth (below 7.3 dB return loss) are overlap each other to achieve a desirable CP antenna design.

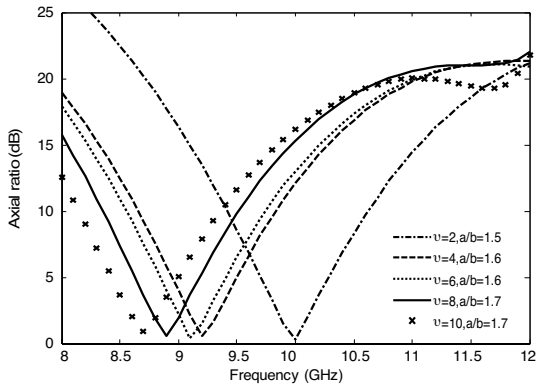

Figure 13. The best axial ratio of superquadric DRA at different squareness parameter.

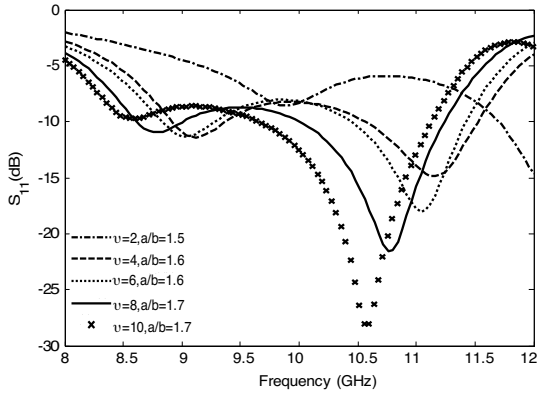

Figure 14. The reflection coefficients corresponding to best axial ratio of Figure 13.

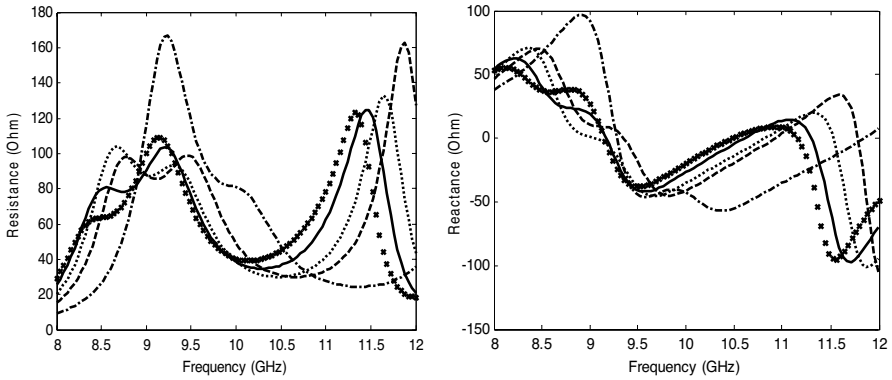

(a) Real part (b) Imaginary part

Figure 15. The input impedance corresponding to best axial ratio of Figure 13.

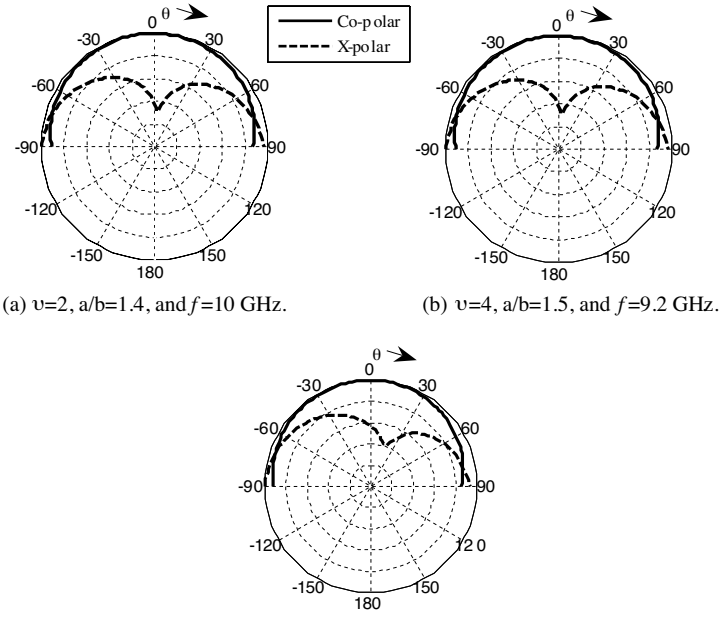

(a) υ=2, a/b=1.4, and f=10 GHz. (b) υ=4, a/b=1.5, and f=9.2 GHz.

(c) υ=10, a/b=1.7, and f= 8.7 GHz.

Figure 16. Computed circular polarization copular and cross-polar radiation patterns at the frequency that has best axial ratio for each case, $h = 4\,\text{mm}$, $L = 3.9\,\text{mm}$.

Table 1 gives the values of aspect ratio (a/b) that gives the best axial ratio and the corresponding resonance frequency (f_r) for each squareness parameter (ν). The aspect ratio (a/b) must be changed with the squareness parameter (ν) to give the desired CP antenna. Figure 11 shows the circular polarization copolar and cross polar radiation patterns plotted at the frequency that has the smallest axial ratio in the direction normal to the antenna ($\theta = 0^\circ$).

Keeping the same dimensions as before and changing the height of the superquadric dielectric resonator antenna "h" = 4 mm and the feeding probe length "ℓ" = 3.9 mm. Figures 12 shows the axial ratio (AR) computed against frequency at different "ν". Also, the resonant frequency decreased as the aspect ratio (a/b) increased when "ν" increased. Figure 13 shows the best axial ratio versus frequency for each "ν" and aspect ratio (a/b). The corresponding reflection coefficient and input impedance for each case are shown in Figures 14 and 15 respectively.

Table 2 gives the values of aspect ratio (a/b) that gives the best axial ratio and the corresponding resonance frequency (f_r) for each squareness parameter (ν). Figure 16 shows the circular polarization copolar and cross polar radiation patterns plotted at the frequency that has the smallest axial ratio in the direction normal to the antenna ($\theta = 0^\circ$).

5. CONCLUSION

Finite element method is used to calculate the dimensions of the superquadric dielectric resonator antenna designed for circular polarization. As the aspect ratio (a/b) increased, with "b" constant, means that the dimension "a" is increased which obviously leading to a lower resonant frequency. For the same aspect ratio (a/b), increasing the squareness parameter (ν) leads to an increase in the volume of the cylinder with both "a" and "b" are kept constant, which also leads to a decrease in the resonant frequency of the cylinder. It became clear from the results that, the aspect ratio (a/b) must be varied with changing the squareness parameter (ν) to achieve a desirable CP antenna design. Also, there is always a frequency at which a relatively good polarization ratio is obtained for ($a/b > 1.3$).

REFERENCES

1. Luk, K. M. and K. W. Leung, *Dielectric Resonator Antenna*, Research Studies Press Ltd., Baldock, Hertfordshire, England, 2003.

2. Al-Zoubi, A. S., A. A. Kishk, and A. W. Glisson, "Analysis and design of a rectangular dielectric resonator antenna fed by dielectric image line through narrow slots," *Progress In Electromagnetics Research*, PIER 77 , 379–390, 2007.
3. Ain, M. F., S. I. S. Hassan, J. S. Mandeep, M. A. Othman, B. M. Nawang, S. Sreekantan, D. Hutagalung, and A. Z. Ahmad, "2.5 GHz $BaTiO_3$ dielectric resonator antenna," *Progress In Electromagnetics Research*, PIER 76 , 201–210, 2007.
4. Fayad, H. and P. Record, "Multi-feed dielectric resonator antenna with reconfigurable radiation pattern," *Progress In Electromagnetics Research*, PIER 76, 341–356, 2007.
5. Zandi, O., Z. Atlasbaf, and K. Forooraghi, "Flat multylayer dielectric reflector antennas," *Progress In Electromagnetics Research*, PIER 72, 1–19, 2007.
6. Mongia, R. K., "Half-split dielectric resonator placed on metallic plane for antenna applications," *Electron. Lett.*, Vol. 35, No. 7, 462–464, Mar. 1989.
7. Ittipiboon, A., R. K. Mongia, Y. M. M. Antar, P. Bhartia, and M. Cuhaci, "Aperture fed rectangular and triangular dielectric resonators for use as magnetic dipole antennas," *Electron. Lett.*, Vol. 29, No. 23, 2001–2002, Nov. 1993.
8. Kishk, A. A., Y. Yin, and A. W. Glisson, "Conical dielectric resonator antennas for wideband applications," *IEEE Trans. Antennas Propag.*, Vol. 50, No. 4, 469–474, Apr. 2002.
9. Kishk, A. A., "Tetrahedron and triangular dielectric resonator antenna with wideband performance," *Proc. IEEE Antennas and Propagation Int. Symp.*, Vol. 4, 262–265, June 2002.
10. Junker, G. P., A. A. Kishk, and A. W. Glisson, "Input impedance of dielectric resonator antennas excited by a coaxial probe," *IEEE Trans. Antennas Propag.*, Vol. 42, No. 7, 960–966, July 1994.
11. St-Martin, J. T. H., Y. M. M. Antar, A. A. Kishk, A. Ittipiboon, and M. Cuhaci, "Dielectric resonator antenna using slot-coupling," *Electron. Lett.*, Vol. 26, No. 24, 1016–2015, Nov. 1990.
12. Petosa, A., R. K. Mongia, A. Ittipiboon, and J. S. Wight, "Design of microstrip fed series array of dielectric resonator antennas," *Electron. Lett.*, Vol. 31, No. 16, 1306–1307, Aug. 1995.
13. Al Salameh, M. S. and Y. M. M. Antar, "Coplanar-waveguide-fed slot coupled rectangular dielectric resonator antenna," *IEEE Trans. Antennas Propag.*, Vol. 50, No. 10, 1415–1419, Oct. 2002.
14. Huang, C. Y., J. Y. Wu, and K. L. Wong, "Cross-slot coupled microstip antenna and dielectric resonator antenna for circular

polarization," *IEEE Trans. Antennas Propag.*, Vol. 47, No. 4, 605–609, Apr. 1999.

15. Kisk, A., "An elliptical dielectric resonator antenna designed for circular polarization with single feed," *Microwave and Optical Technology Letters*, Vol. 37, No. 6, 454–456, June 2003.
16. Dong, X. and T. An, "A new FEM approach for open boundary Laplace's problem," *IEEE Trans. Microw. Theory Tech.*, Vol. 44, 157–160, Jan. 1996.
17. Zhou, X. and G. W. Pan, "Application of Physical Spline Finite Element Method (PSFEM) to full wave analysis of waveguide," *Progress In Electromagnetics Research*, PIER 60, 19–41, 2006.
18. Gavrilovic, M. M. and J. P. Webb, "Accuracy control in the optimization of microwave devices by finite element methods," *IEEE Trans. Microw. Theory Tech.*, Vol. 50, No. 8, 1901–1911, Aug. 2002.
19. Pingenot, J., R. N. Rieben, D. A. White, and D. G. Dudley, "Full wave analysis of RF signal attenuation in a lossy rough surface cave using a high order time domain vector finite element method," *J. of Electromagn. Waves and Appl.*, Vol. 20, No. 12, 1695–1705, 2006.
20. Hernandez-Lopez, M. A. and M. Quintillan-Gonzalez, "A finite element method code to analyse waveguide dispersion," *J. of Electromagn. Waves and Appl.*, Vol. 21, No. 3, 397–408, 2007.
21. Mitchell, A., D. M. Kokotoff, and M. W. Austin, "Improvement to the PML boundary condition in the FEM using mesh compression," *IEEE Trans. Microw. Theory Tech.*, Vol. 50, No. 5, 1297–1302, May 2002.
22. Harscher, P., S. Amari, and R. Vahldieck, "A fast finite-element-based field optimizer using analytically calculated gradients," *IEEE Trans. Microw. Theory Tech.*, Vol. 50, No. 2, 433–439, Feb. 2002.
23. Jensen, M. A. and Y. Rahmat-Samii, "Electromagnetic characteristics of superquadric wire loop antennas," *IEEE Trans. Antennas Propagat.*, Vol. 42, No. 2, 264–269, Feb. 1994.
24. Wong, K. L., *Planar Antenna for Wireless Communication*, Wiley, New York, 2003.